fluids

MDPI

Article

Experimental Correlation for Splashing Condition of Droplets on Solid Substrates

Yukihiro Yonemoto [1,*], Kanta Tashiro [2], Minori Yamashita [2] and Tomoaki Kunugi [3,*]

[1] Division of Industrial Fundamentals, Faculty of Advanced Science and Technology, Kumamoto University, 2-39-1, Kurokami, Chuo-ku, Kumamoto-shi, Kumamoto 860-8555, Japan
[2] Department of Mechanical and Mathematical Engineering, Kumamoto University, 2-39-1, Kurokami, Chuo-ku, Kumamoto-shi, Kumamoto 860-8555, Japan; 202d3118@st.kumamoto-u.ac.jp (K.T.); 213d8529@st.kumamoto-u.ac.jp (M.Y.)
[3] College of Energy Engineering, Zhejiang University, 38 Zheda Road, Hangzhou 310027, China
* Correspondence: yonemoto@mech.kumamoto-u.ac.jp (Y.Y.); kunugi.tomoaki.85s@st.kyoto-u.ac.jp (T.K.)

Abstract: Droplet splashing behaviors of water-ethanol binary mixture liquids on roughened solid surfaces were experimentally observed in order to investigate the effects of surface tension, viscosity, and wettability/surface roughness on the splashing occurrence. The range of the droplet volumes was from 1.7 μL to 32.6 μL. The ranges of the surface tension and the viscosity were from 21.1 mN/m to 71.9 mN/m, and from 1 mPas to 2.91 mPas, respectively. The surface roughness range was from 0.03 μm to 1.25 μm for R_a. The present experimental data were evaluated on the basis of the existing models. Resulting from these experiments, a simple model using the Ohnesorge number evaluated by the capillary length was proposed and the accuracy of the predicted critical values such as the critical Weber and Reynolds numbers were discussed. The result indicated that the liquid properties and the quantification of the surface condition such as surface roughness are important factors for the prediction of the splashing behavior.

Keywords: droplet; splashing; wettability; surface roughness

Citation: Yonemoto, Y.; Tashiro, K.; Yamashita, M.; Kunugi, T. Experimental Correlation for Splashing Condition of Droplets on Solid Substrates. *Fluids* **2022**, *7*, 38. https://doi.org/10.3390/fluids7010038

Academic Editor: Mehrdad Massoudi

Received: 17 November 2021
Accepted: 12 January 2022
Published: 16 January 2022

1. Introduction

Droplet behavior is very simple and fundamental. However, droplet behavior has great potential to applications in a variety of industrial, agricultural, medical, and biological fields. Especially, droplet impingement behavior is related to inkjet printing [1], spray cooling [2,3], spray painting [4], fuel injection [5], and pesticide spray in agriculture [6] and so on. In such applications, the precise predictions of the droplet behaviors such as the spreading size of the droplet, the contact time between liquid and solid surface during the impingement process and splashing or not are very important for an estimation of effective heat transfer, efficient consumption of the pesticide, coating material, and the inkjet process. The droplet impingement process exhibits a variety of behaviors depending on the competition among the impingement kinetic energy, surface energy contribution, viscous dissipation, and so on. The behavior is mainly classified into three processes such as the deposition, spreading with surface instability such as a finger, and splash with a secondary droplet from the tip of the liquid film [7]. As to the deposition process, at the present time, there are many studies for the prediction of the dimensionless maximum spreading diameter called the spreading factor β_m (= d_{max}/d_0: d_{max} is the maximum spreading diameter, d_0 is the initial droplet diameter) from the experimental, numerical, and theoretical [8–17] point of views, although β_m includes the definition of both contact area diameter and the diameter between the rim edges in some literature [18]. However, there are many unclear points for the droplet splashing behavior in spite of many efforts of experimental, numerical, and theoretical studies. Thus, the prediction of the droplet splashing behavior depends on the empirical approach and is still an open question.

From the experimental point of view, various empirical models for the prediction of the splashing condition were proposed [19–23]. The splashing parameter $K = \mathrm{OhRe}^{1.25}$ is a famous model for the prediction of the splashing occurrence [24]: Oh is the Ohnesorge number ($=\mathrm{We}^{1/2}\mathrm{Re}^{-1}$), and We ($=\rho_l u^2 d_0/\sigma_{lg}$) and Re ($=\rho_l u d_0/\mu_l$) are the Weber and Reynolds numbers, respectively: ρ_l is liquid density, μ_l is liquid viscosity, u is impingement velocity, and σ_{lg} is surface tension. In this model, the droplet splashing behavior can be judged whether the value of K exceeds 57.7 or not. This model was developed on the basis of the splashing behaviors for a few kinds of liquid droplets impinging on stainless steel surfaces. However, in an actual situation, the droplet splashing behavior is affected by the surface condition such as the surface roughness. In subsequent studies, various models that include the surface roughness factors such as the arithmetical mean roughness value (R_a) and the mean peak width (R_{sm}), and so on, have been proposed [25,26]. In the recent theoretical approach, local liquid film behavior was thoughtfully discussed and the model with a balance among the vertical lift force acting on the edge of the lamella, the suction forces due to gas, and the retraction force by capillary was proposed [27–29]. In this model, the angle of rim edge lifted up was a key parameter. In addition to the surface roughness factor, it was reported that the surface wettability also affected droplet splashing behaviors [30]. However, at present, there is still a lack of general understanding of the droplet splashing behavior because of its complexity, although our knowledge of the behavior would gradually proceed toward understanding the mechanism by the local consideration of the liquid film behavior.

In the present study, droplet splashing behaviors were experimentally investigated in order to understand the effects of liquid properties (surface tension and viscosity), wettability, solid surface roughness, and droplet volume on the splashing occurrence. Then, the experimental data were evaluated by some existing models, a simple model using Oh evaluated by the capillary length was proposed, and the validity and the applicability of all the models were discussed. The present result implies the importance of the liquid property, wettability, and the quantification of the solid surface roughness for the splashing behavior.

2. Materials and Methods

The droplet splashing behaviors on the solid substrates were measured using a high-speed video camera with 20,000 fps (HX-5, NAC image technology, Ltd., Tokyo, Japan) with a microscope (Leica Microsystems, Welzlar, Germany) or a microlens (Nikon AF-S VR Micro-Nikkor 105 mm f/2.8G IF-ED, Tokyo, Japan). The point of view of the camera is about 4 (deg.). In the present experiment, water-ethanol binary mixtures were used as the liquid sample. The mass concentration was varied from 0 wt% to 99.4 wt% ethanol (ultrapure water; Wako Pure Chemical Industries, Ltd., Osaka, Japan, 0 wt%, pure ethanol; Nacalai Tesque, Inc., Kyoto, Japan, 99.4 wt% pure). The droplet was gently released without the initial velocity using a microsyringe from several release heights, z = 5 mm to 2400 mm. The range of the droplet impingement velocity is 0.28 m/s to 5.38 m/s in the present study. The impingement velocity was measured from captured images by high-speed video camera (Section S1 in the Supplementary Materials). The droplet volume ranged from 1.9 µL to 32.2 µL. The initial droplet diameter d_0 was evaluated by the captured image where the sphere equivalent diameter is considered assuming the ellipsoid as $2({r_{0h}}^2 r_{0v})^{1/3}$: the vertical ($r_{0v}$) and horizontal ($r_{0h}$) radii for the falling droplet. The droplet volumes were controlled using three kinds of syringes. Concretely speaking, small- and medium-sized droplets are released using 32G and 22G stainless steel needles (Kyowa Interface Science Co., Ltd., Saitama, Japan) attached to the syringe (SS-02LZ, Terumo Co., Tokyo, Japan), respectively. The large-sized droplet is released using the syringe without the needle. The range of the measured initial droplet diameters are 2.0–3.9 mm for 0 wt%, 1.9–3.6 mm for 5 wt%, 1.7–3.5 mm for 20 wt%, 1.5–3.4 mm for 40 wt%, 1.6–3.4 mm for 70 wt%, and 1.5–3.5 mm for 99.4 wt%. Here, the size was measured using the analysis software LAA Measurement2 (NAC image technology, Ltd., Tokyo, Japan) and the maximum error was ±0.032 mm. The surface tensions of the liquids were measured using a DM300 (Kyowa

Interface Science Co., Ltd., Saitama, Japan). The contact angle was measured using the analysis software FAMAS (Kyowa Interface Science Co., Ltd., Saitama, Japan) equipped with the tangent method. The liquid physical properties of the density ρ_l [kgm^{-3}], viscosity μ_l [mPas] and surface tension σ_{lg} [Nm^{-1}] are 998.2, 1.00, and 0.0719 for 0 wt%, 987.7, 1.25, and 0.0563 for 5 wt%, 967.0, 2.18, and 0.0384 for 20 wt%, 935.0, 2.91, and 0.0300 for 40 wt%, 864.9, 2.37, and 0.0256 for 70 wt%, and 789.2, 1.20, and 0.0211 for 99.4 wt%, respectively. Here, the liquid density was measured using the portable density/specific gravity meter (DA-130N, Kyoto electronics manufacturing Co., Ltd., Kyoto, Japan). For the values for the liquid viscosity, the literature data were used [31]. For solid materials, polycarbonate (PC) was used. The surface of the test material was polished in order to consider the effect of the surface roughness on the droplet behavior using a grinder-polisher (MetaServ^{TM}250 Grinder-Polisher, Buehler Ltd., Lake Bluff, IL, USA) and four kinds of solid substrates with different surface roughness polished by Grit #400 (408-400AU), #240 (408-240AU) and #120 (408-120AU) (Sankei Co. Ltd., Tokyo, Japan) were finally prepared. The bare surface which was not polished was also used as the test material. The surface morphological conditions were measured with a laser scanning microscope (LEXT OLS4100, Olympus Co. Ltd., Tokyo, Japan). In the present study, R_a and R_{sm} were mainly measured as shown in Table 1.

Table 1. Solid surface conditions. The arithmetical mean roughness value (R_a) (μm) and the mean peak width (R_{sm}) (μm) for each solid substrate.

	Bare	**#400**	**#240**	**#120**
R_a (μm)	0.03	0.33	0.99	1.25
R_{sm} (μm)	2.91	8.03	13.9	15.1

Each condition at the same release height was performed three times. The splashing was determined when an ejected secondary droplet was observed three times from the same release height. The increment of the release height is 10 mm. Temperature and relative humidity were kept in the range of 20.0–25.0 °C and 50.0–55.0%, respectively. The detailed information is shown in Table 2.

Table 2. Temperature (°C) and relative humidity (RH) (%) in the present experiment.

wt (%)	**Temperature**	**RH**
0	20.7–24.7	50.0–55.0
5	21.5–25.0	50.0–54.9
20	21.3–24.0	50.1–55.0
40	21.5–23.9	50.1–54.9
70	21.4–24.4	50.1–55.0
99.4	20.9–24.2	50.0–54.9

3. Existing Model for Splash Condition

In the present study, the experimental data were evaluated by the existing splashing model. Concretely speaking, the model proposed by Garcia-Geijo et al. and Gordillo and Riboux [27–29] was applied for the present experimental data. The model mainly considers the local liquid–film behavior in the splashing process. In their recent study [28], the splashing model is categorized depending on the wettability and the surface roughness condition which is judged by the newly defined We number characterized by the grit size of the sandpaper ε as $We_\varepsilon = \rho_l u^2 \varepsilon / \sigma$. According to their model, if $We_\varepsilon \leq 1$, there are two splashing models that account for hydrophilic-like behavior and hydrophobic-like behavior. If $We_\varepsilon \geq 1$ and the liquid wets the substrate, a new correlation is proposed such as $We_c \propto (r_0 \cos\theta_0 / \varepsilon)^{3/5}$: r_0 is the initial droplet radius and θ_0 is the static contact angle. In the present study, all experimental conditions held the condition of $We_\varepsilon \leq 1$, and the combination between water-ethanol mixture liquids and the PC substrate exhibited

a relatively hydrophilic tendency. Here, the values for ε in the present experiment were evaluated using the following relation [28].

$$R_a = 0.943 + 0.134\varepsilon \qquad \text{for } R_a \geq 1\ \mu m \tag{1a}$$

$$R_a = \varepsilon \qquad \text{for } R_a < 1\ \mu m \tag{1b}$$

Equation (1a,b) represent the relationship between the grit size ε and the R_a on the sandpaper. In the present study, the droplet impinges not on the sandpaper but the solid substrate polished by sandpapers. Therefore, the values of ε for the solid substrates used in the present study were deduced from Equation (1a,b) because the values of R_a for bare, #400, #240, and #120 substrates were known. The evaluated values of ε were 0.03 μm for the bare, 0.33 μm for #400, 0.99 μm for #240, and 2.29 μm for #120 substrates.

In the hydrophilic case, the critical condition for the onset of the splashing regime is given by the following equations [28] that are developed on the basis of the concept where the vertical velocity of the edge of the expanding liquid sheet becomes larger than the radial growth of the rim [29].

$$K_c = K_l \left(\frac{\mu_g}{\mu_l}\right) \mathrm{Oh_{RG}} \mathrm{We_{RG}^{5/6}} \tag{2}$$

$$K_l = \frac{3}{\tan^2 \alpha} \ln\left[A \left(\frac{\mu_l}{\mu_g}\right)^{3/4} \mathrm{Oh_{RG}^{-1/4}} \left(\mathrm{We_{RG}} \frac{\lambda_g}{r_0}\right)^{-1}\right] \tag{3}$$

The above equations were applied to our experimental data. In this model, We and Oh numbers were defined using the characteristic length as the initial droplet radius r_0. Therefore, the expressions of $\mathrm{We_{RG}}$ and $\mathrm{Oh_{RG}}$ were used to distinguish them with other We and Oh as in Equations (4), (12), and (16). μ_g, μ_l, u, σ_{lg}, and λ_g are the gas and liquid viscosities, droplet impingement velocity, surface tension and the mean free path of gas molecules, respectively. A and α are the fitting constant [29] and the lifted angle of the rim tip of the liquid film, respectively. The droplet splashing occurred when $K_c \simeq 0.034$ [29]. Here, the value of A was set as 0.011. In addition, it was reported that the value of α was 60 ± 3.6 (deg.) and the value perfectly reproduced the experimental impingement velocity where the splashing occurs [27,29] although the value was slightly influenced by wetting properties of the solid surface [29]. Therefore, in the present study, α was set as 60 (deg.). However, in an actual situation, the observed lifted angle of the liquid film seems to be less than 60 (deg.) in the prompt splashing behavior [32], even if the wettability affects the splashing behavior. In addition, although the effect of the surface roughness on the splashing is categorized using $\mathrm{We_\varepsilon}$, the categorization condition for the effect of the wettability such as hydrophilic-like or hydrophobic-like behavior is ambiguous. This means that the model lacks the information about the wettability. If the model in Equation (2) can capture the physics of the splashing behavior, the splashing condition would be explained by a single model without complex categorization. Therefore, in the present study, the relationship between the wettability and the lifted angle of the liquid film was mainly considered in the evaluation of Equation (2).

Then, in addition to the above model, the empirical relation proposed by Tang et al. [33] was also applied in order to consider the applicability for the present study. This model basically focused on the splashing behavior for de-ionized water, ethanol, decane, and tetradecane as test liquids on five standard reference specimens. Initial droplet diameters ranged from 1.89 to 2.64 mm. In the reference [33], the empirical correlation for the dimensionless maximum spreading contact area diameter was also proposed as $\beta_m \propto (\mathrm{We/Oh})^n$. The following splashing model was finally developed based on the concept where the maximum spreading behavior could characterize the splashing behavior.

$$K_t = \left(\frac{\mathrm{We}}{\mathrm{Oh}}\right)^{1/2} = C + D \ln\left(\frac{R_a}{d_0}\right) \tag{4}$$

In Equation (4), C and D are fitting parameters defined for the kinds of liquids [33]. Unlike Equation (2), this model does not consider the physics of the liquid film behavior, but explicitly focuses on the effect of the surface roughness on the splashing condition. Therefore, the model does not consider the effect of the liquid properties on droplet conditions such as the size of droplet and wettability on the splashing behavior. In the present study, Equation (4) was evaluated by focusing on the effects of those parameters on C and D.

Furthermore, the relation of $\mathrm{OhRe^n} = \mathrm{C_0}$ was applied to the present experimental results because it was reported that the approach considering Re and Oh exhibited strong correlation for the smooth and rough solid substrate [24].

4. Result and Discussion

4.1. Droplet Spreading in Deposition Process

Figure 1 shows the time evolution of the dimensionless contact area diameter $\beta(t)$ (the contact area diameter d_{cont} (t)) normalized by the initial droplet diameter (d_0) for purified water (0 wt%) and water-ethanol binary mixture liquid (70 wt%) on bare and #400 substrate in the deposition process, respectively. Figure 1a,c represent overview images for 0 wt% and 70 wt%, respectively. Then, Figure 1b,d represent the magnified image in Figure 1c, respectively. The release heights of droplets are 5 mm, 10 mm, 50 mm, and 100 mm. In Figure 1b,d, the red points represent the stationary points where the gradient of $\mathrm{d}\beta(t)/\mathrm{d}t \approx 0$. Here, the stationary point is determined by considering the gradient of $\mathrm{d}\beta(t)/\mathrm{d}t$ before and after the time t. If the averaged value of $|(\beta(t) - \beta(t - \Delta t))/\Delta t|$ and $|(\beta(t) - \beta(t + \Delta t))/\Delta t|$ approximately takes zero, the point is determined as the stationary point in addition to the consideration of the behavior for $\beta(t)$. However, note that the determination includes the size measurement error due to the image processing. A typical image for droplet behavior after the impingement is that the tip of the liquid film spreads over the solid surface in the radial direction, and the contact area radius reaches the maximum value. After that, the retraction behavior starts and the contact area radius recedes. Finally, the droplet reaches the equilibrium state. The case of 0 wt% exhibits this kind of behavior as shown in Figure 1a,b. However, in the case of 70 wt%, the contact area diameter gradually spreads over the solid surface after reaching the stationary points. This may be related to the morphological effect on the wettability at the contact line. The liquid near the contact line infiltrates into the microstructure on the solid surface. Although this tendency may be influenced by the competition against the fluid flow near the contact line, the spreading tendency becomes large depending on the strength for the wettability [34,35]. Thus, due to the strong adhesion, it is hard for the retraction process to occur. This induces gradual spreading as the spreading process changes from the inertial dominated one (before the red point) to the wettability dominated one (after the red point). Similar behaviors were observed in other liquid cases, and even in the bare substrate if the adhesion strength is very large.

4.2. Droplet Splashing Behavior

Figure 2 shows the sample images for the droplet splashing. Figure 2a–c show the images for the cases of 0 wt% on the bare and #400 substrates, and 99.4 wt% on the bare substrate, respectively. In Figure 2, the droplet volumes for water and 99.4 wt% were 4.5 µL and 4.8 µL, respectively. From the figures, it is found that the liquid film arises just after the droplet impingement on the solid surface. Then, the secondary droplet indicated by the dashed red circle is ejected from the tip of the liquid film. From the observation of the droplet splashing behaviors, the critical We number ($\mathrm{We_c} = \rho_l {u_c}^2 d_0/\sigma_{lg}$) and Re number ($\mathrm{Re_c} = \rho_l u_c d_0/\mu_l$) were determined.

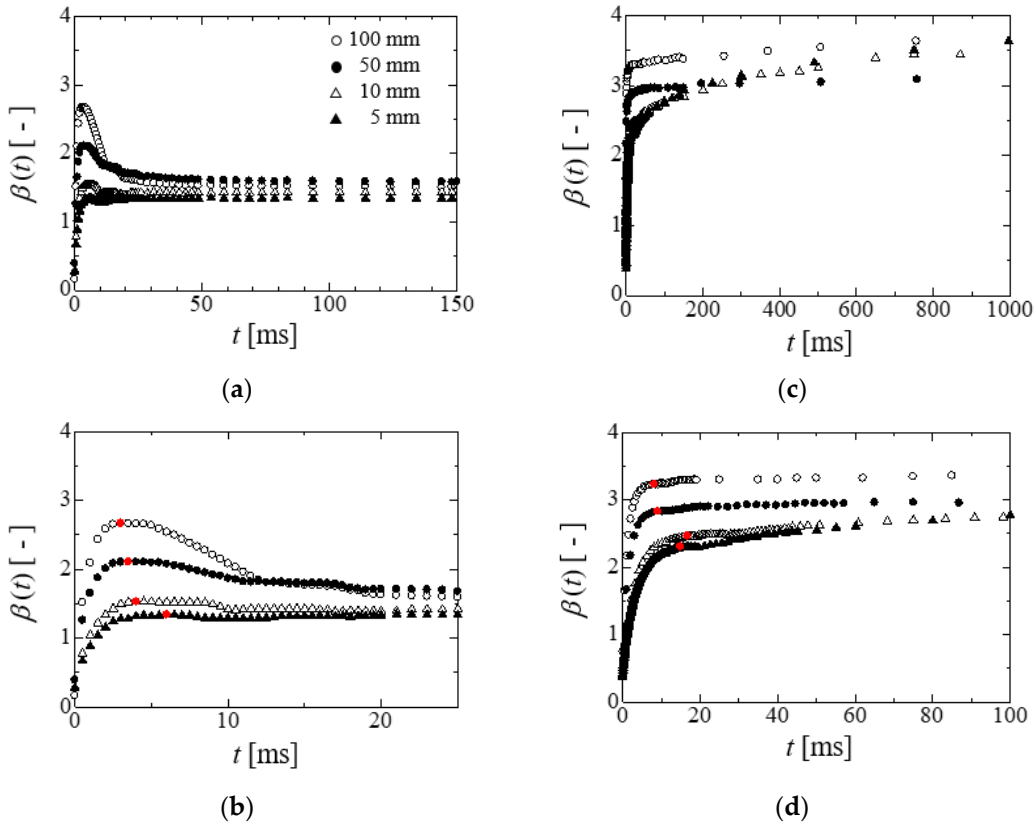

Figure 1. Time evolution of dimensionless contact area diameter $\beta(t)$: (**a**) 0 wt% on bare substrate; (**b**) magnified image for 0 wt% on bare substrate in (**a**); (**c**) 70 wt% on #400 substrate; and (**d**) magnified image for 70 wt% on #400 substrate in (**c**).

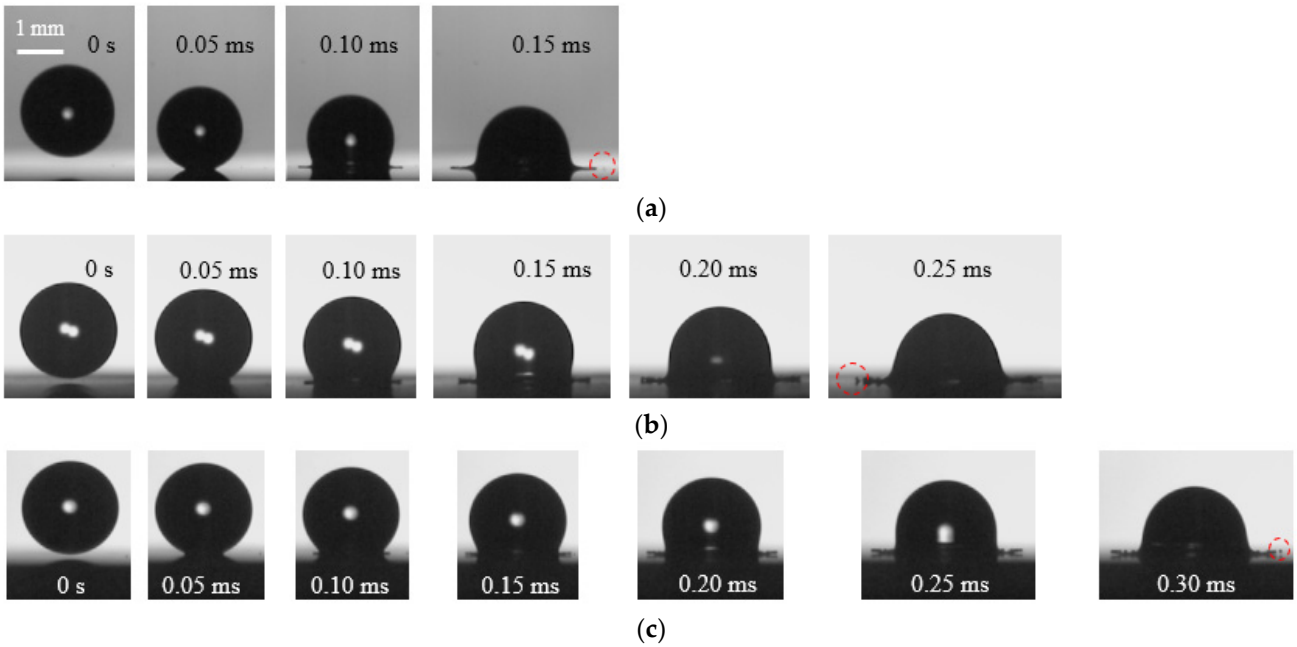

Figure 2. Splashing images of droplets on solid substrates: (**a**) 0 wt% droplet on bare substrate; (**b**) 0 wt% on #400 substrate; and (**c**) 99.4 wt% substrate. Droplet volumes are 4.5 µL for water and 4.8 µL for 99.4 wt%. The red dashed circle represents the firstly ejected secondary droplet from the rim of the liquid film.

From these figures, it is also found that the tip of the liquid film is lifted up in the upward direction. Although it was very difficult to measure the lifted angle from the solid surface in some cases as shown in the case of 0 wt% (Figure 2a), some examples are shown in Figure 3. The lifted angles are less than 20 (deg.). These values are a large discrepancy from the value used in Equation (2). Actually, it may be very difficult to determine the lifted angle because the contact angles also have some definitions such as microscopic and macroscopic contact angles [36]. The lifted angle may also have the same characteristic. At least, the apparently lifted angle was less than 60 (deg.) in the present study.

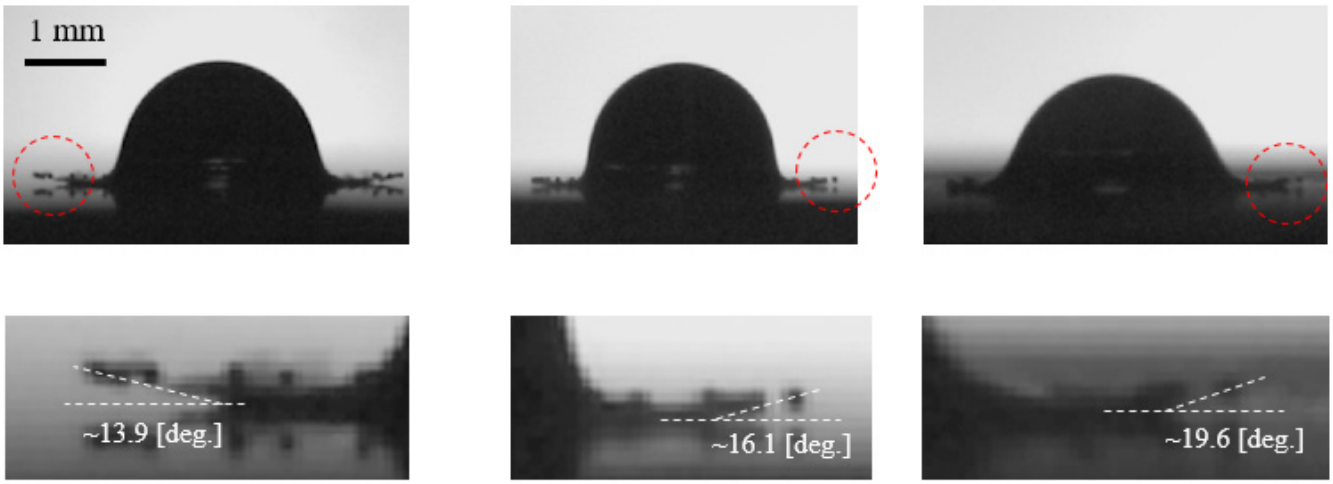

Figure 3. Lifted angle of the liquid film: (**a**) 20 wt% droplet on bare substrate; (**b**) 99.4 wt% on bare substrate; and (**c**) 99.4 wt% on #240 substrate.

4.3. Evaluation of Experimental Result for Droplet Splashing Behavior

Figure 4 shows the relationship between K_c and the mass concentration of water-ethanol binary mixture liquids for each solid substrate. The red solid line represents the splashing condition of $K_c \simeq 0.034$. From the result for the bare substrate, it is found that the calculated values for K_c show relatively good agreement with the splashing condition. However, in other cases for #400, #240, and #120, there are large deviations from $K_c \simeq 0.034$. With respect to the splashing behavior, the wettability dependence for the splashing condition was reported [26,30]. In the splashing model in Equations (2) and (3), there are no parameters to consider the wettability except for α. At least, the deposition process could be influenced by the wettability and the surface roughness, so the K_c values would be influenced by the surface condition. In fact, the lifted angle observed in the present experiment was not around the value of 60 (deg.). This may imply that the modification of the parameter is related to α, such as $\tan\alpha_{mod} = f(\theta)\tan\alpha$. Furthermore, the calculated values of K_c have distribution to a certain extent, which indicates the effect of the droplet volume on the splashing condition. The lift force exerted by the gas on the edge of the expanding lamella is related to the slip length at the gas–liquid interface which is considered in K_l and is approximately proportional to $Oh_{RG}{}^{1/4}$ [29]. However, the lift force would be influenced by the droplet volume because the film thickness is also influenced by the droplet volume.

Figure 5 shows the relationship between the contact angle and the $K_c \cdot (r^*)^{1/4}$ values in each solid substrate. Here, r^* is the initial droplet radius r_0 normalized by the capillary length l_{cap} of the liquid: $r^* = r_0/l_{cap}$ and $l_{cap} = (\sigma_{lg}/(\rho_l g))^{1/2}$. r^* implicitly represents the effect of the gravity on the splashing because of $(r^*)^2$~Bond number evaluated by the initial droplet radius as Bo_{RG} ($=\rho_l g {r_0}^2/\sigma_{lg}$). The contact angle $\bar{\theta}_{ave}$ was evaluated by averaging the static contact angle θ_{static} [34] and the contact angle at the stationary point θ_{stat} where

the dimensionless contact area diameter reached the stationary condition ($d\beta(t)/dt \approx 0$) after the impingement in the deposition process as shown in Figure 1. Here, Figure 6 shows examples for the snapshots of droplets at the stationary point of 40 wt% on bare substrate released from 5 mm, 10 mm, and 50 mm height. The contact angle at the stationary point is measured using the images for this kind of snapshot. As an example, the trend of the contact angles ($1 + \cos\bar{\theta}_{ave}$) against the ethanol concentration are shown in Figure 7. Actual values of $\cos\bar{\theta}_{ave}$ are shown in Table 3. It is found that the figure exhibits a strong correlation between the $K_c \cdot (r^*)^{1/4}$ value and the contact angle. This tendency implies the following relation:

$$K_c \cdot (r^*)^{1/4} = a(1 + \cos\bar{\theta}_{ave}) + b \quad (5)$$

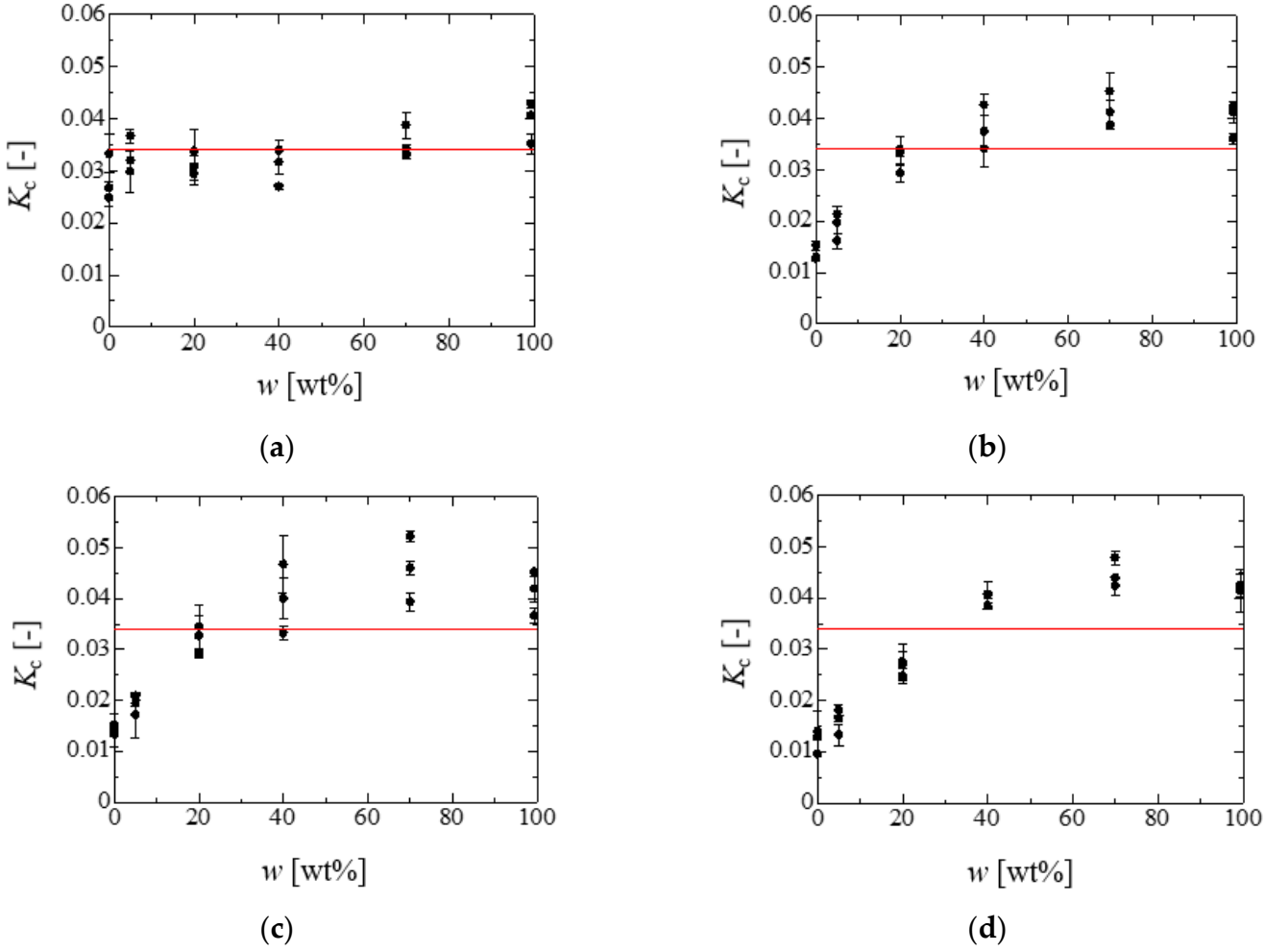

Figure 4. Splashing condition K_c calculated by Equations (1) and (2) in each liquid: (**a**) bare substrate; (**b**) #400 substrate; (**c**) #240 substrate; and (**d**) #120 substrate. The splashing occurrence is defined by $K_c \simeq 0.034$ (red solid line) [28,29]. The error indicates two standard deviation (2SD).

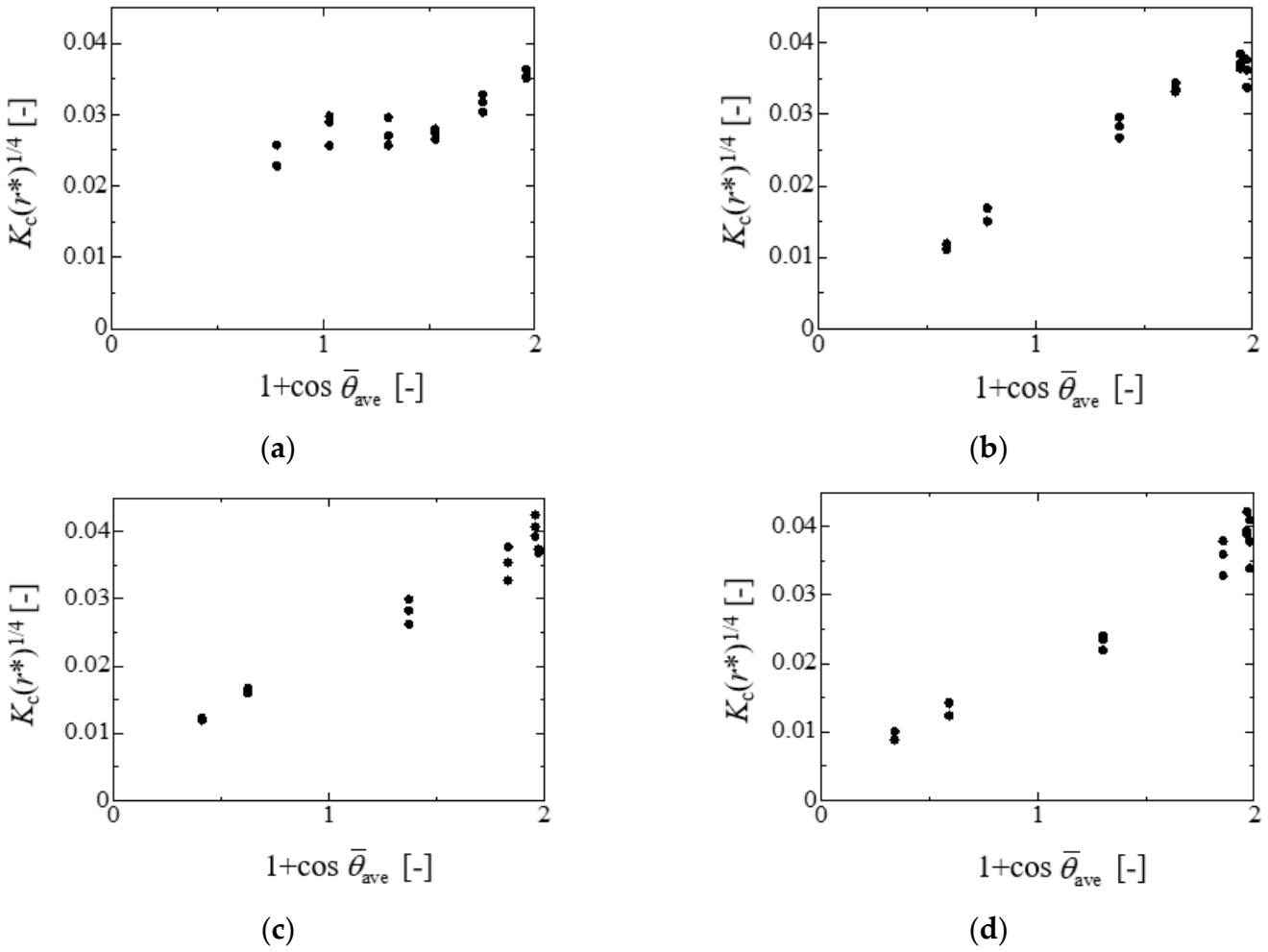

Figure 5. Relationship between the splashing condition K_c and the contact angle: (**a**) bare substrate; (**b**) #400 substrate; (**c**) #240 substrate; and (**d**) #120 substrate. The contact angle $\bar{\theta}_{ave}$ is calculated by averaging the static contact angle and the contact angle where the dimensionless contact area diameter reaches the stationary condition after the impingement.

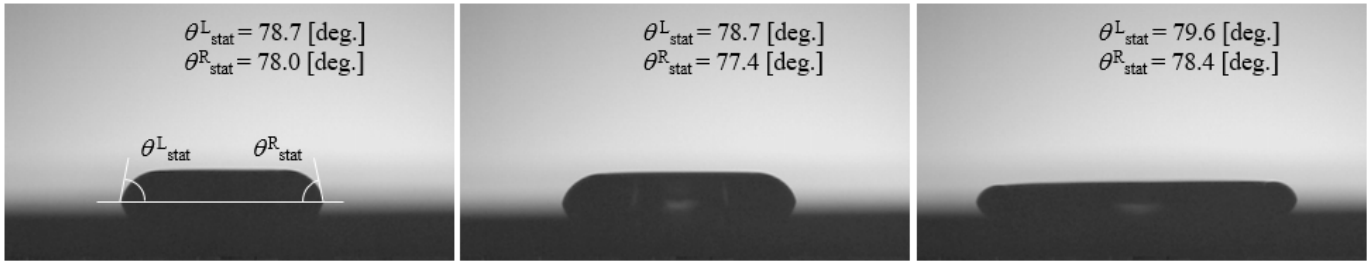

Figure 6. Example of contact angle at the stationary point θ_{stat} for 40 wt% droplets (5.7 μL) on bare substrate. Snapshots of droplets released from (**a**) 5mm, (**b**) 10 mm, and (**c**) 50 mm height. θ_{stat} is evaluated by simple averaging procedure as $(\theta^L_{stat} + \theta^R_{stat})/2$.

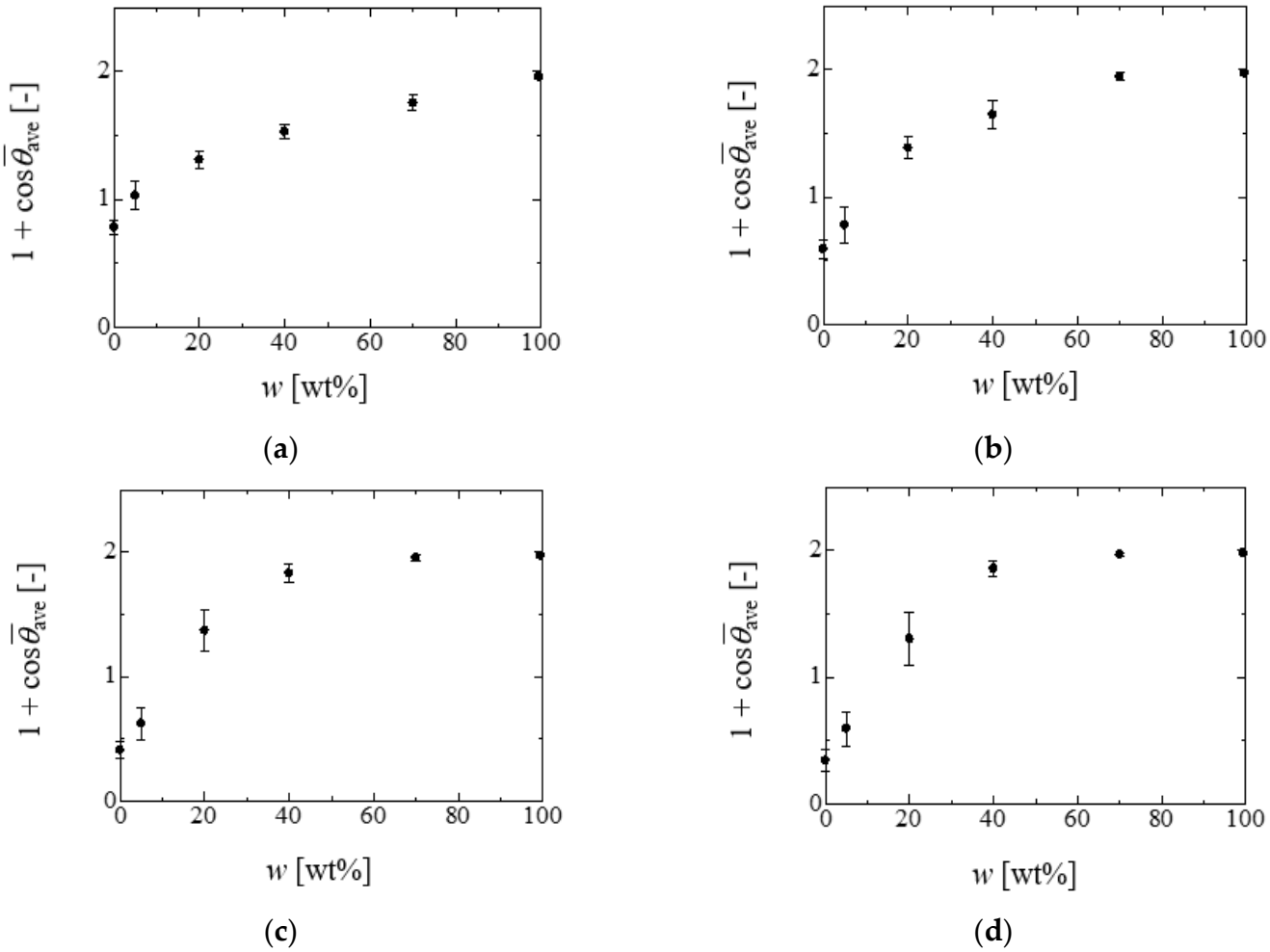

Figure 7. Relationship between 1 + cos$\overline{\theta}_{ave}$ and the mass concentration of ethanol: (**a**) bare substrate; (**b**) #400 substrate; (**c**) #240 substrate; and (**d**) #120 substrate. The error indicates two standard deviation (2SD).

Table 3. Values for cos$\overline{\theta}_{ave}$ in each solid substrate.

	Bare	**#400**	**#240**	**#120**
0 wt%	–0.217	–0.407	–0.589	–0.659
5 wt%	0.031	–0.220	–0.375	–0.407
20 wt%	0.310	0.388	0.371	0.303
40 wt%	0.531	0.647	0.831	0.858
70 wt%	0.756	0.945	0.957	0.968
99.4 wt%	0.961	0.975	0.973	0.982

In this relation, the coefficients a and b can be represented by the following relations through the analysis of their coefficients (Section S2 in the Supplementary Materials):

$$\frac{a - a_{\text{bare}}}{a_{\text{bare}}} = C_{a1}\tanh\left\{C_{a2}\left(\frac{f_{\text{rf}} - f_{\text{rf}}^{\text{Bare}}}{f_{\text{rf}}^{\text{Bare}}}\right)\right\} \quad (6)$$

$$\frac{b_{\text{Bare}} - b}{b_{\text{Bare}}} = C_{b1}\tanh\left\{C_{b2}\left(\frac{f_{\text{rf}} - f_{\text{rf}}^{\text{Bare}}}{f_{\text{rf}}^{\text{Bare}}}\right)\right\} \quad (7)$$

In Equations (6) and (7), a_{bare}, b_{bare}, C_{a1}, C_{a2}, C_{b1}, and C_{b2} represent the arbitral fitting parameters of 8.223×10^{-3}, 1.745×10^{-2}, 1.137, 71.69, 0.8060, and 69.23, respectively. f_{rf} represents the surface roughness factor and is defined by the following relation [34]:

$$f_{rf} = \frac{1 + 4\dfrac{R_a}{R_{sm}}}{1 + 4\dfrac{R_a}{R_{sm}}\Big|_{bare}} \tag{8}$$

Equations (6) and (7) are developed by considering the dependency of the coefficients a and b on the roughness parameter f_{rf} where the bare substrate is treated as the reference condition because the wettability of droplet on solid substrate is basically characterized by the relative relation among solid substrates [34]. If both terms of Equation (5) are divided by $a(1 + \cos\overline{\theta}_{ave}) + b$, the following relation can be obtained.

$$\frac{K_c \cdot (r^*)^{1/4}}{a(1 + \cos\overline{\theta}_{ave}) + b} = 1 \tag{9}$$

The expression in Equation (9) may imply the modification of $\tan\alpha$ into $\tan\alpha\sqrt{a(1 + \cos\overline{\theta}_{ave}) + b}$. Actually, if the modified lifted angle is assumed as α_{mod} and defined as $\tan\alpha_{mod} = \tan\alpha\sqrt{a(1 + \cos\overline{\theta}_{ave}) + b}$ where α = 60 (deg.), the estimated values α_{mod} for the case of (a), (b), and (c) in Figure 3 are 16.2, 17.6, and 18.7 (deg.), respectively. The values of α_{mod} show good agreement with those of the present experimental observations.

Figure 8 shows the comparison of the experimental value for $K_{c\text{-}exp}$ with the predicted one $K_{c\text{-}pre}$ in each solid substrate. From the figure, it is found that the present model in Equation (5) well correlates with the splashing condition.

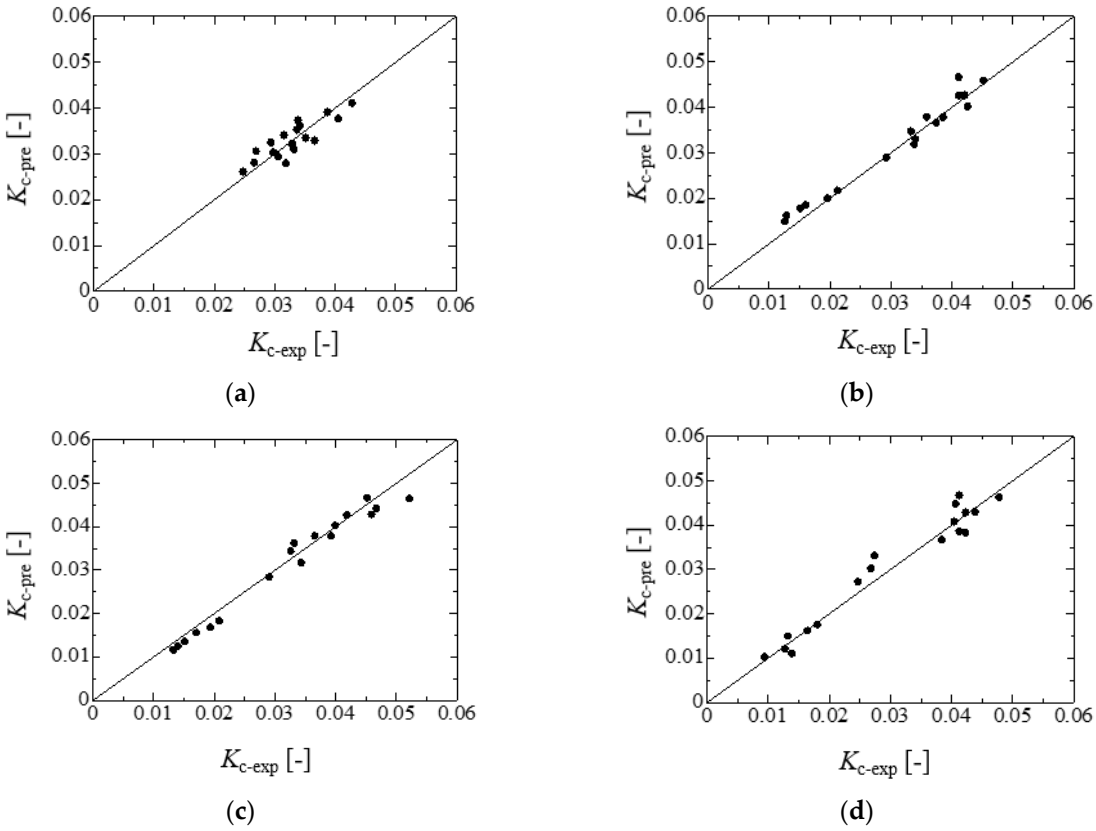

Figure 8. Comparison of $K_{c\text{-}exp}$ with $K_{c\text{-}pre}$: (**a**) bare substrate; (**b**) #400 substrate; (**c**) #240 substrate; and (**d**) #120 substrate. $K_{c\text{-}exp}$ and $K_{c\text{-}pre}$ are evaluated by Equation (2) and Equation (5), respectively.

From here, the applicability of Equation (4) is discussed. Figure 9 shows the examples of the relationship between K_t value and $\ln(R_a/d_0)$ for 5 wt%, 20 wt%, 70 wt%, and 99.4 wt%, respectively. From Figure 9a, it seems that the relationship between K_t and $\ln(R_a/d_0)$ exhibits the linear relation. Actually, two linear relations are mainly observed. For example, as shown in Figure 9c one linearity can be observed from the group depicted by the same symbol. This linearity is related to the change in d_0 (the blue dashed arrow). The other one is observed from three colored solid lines. The black, blue and red solid lines represent small, medium and large-sized droplet volumes, respectively. This linearity is related to the change in R_a (the red dashed arrow). Basically, the model in Equation (4) expresses the linear relationship between K_t and $\ln(R_a/d_0)$ for a single liquid. The effect of the surface roughness on the splashing condition is considered in the term $\ln(R_a/d_0)$.

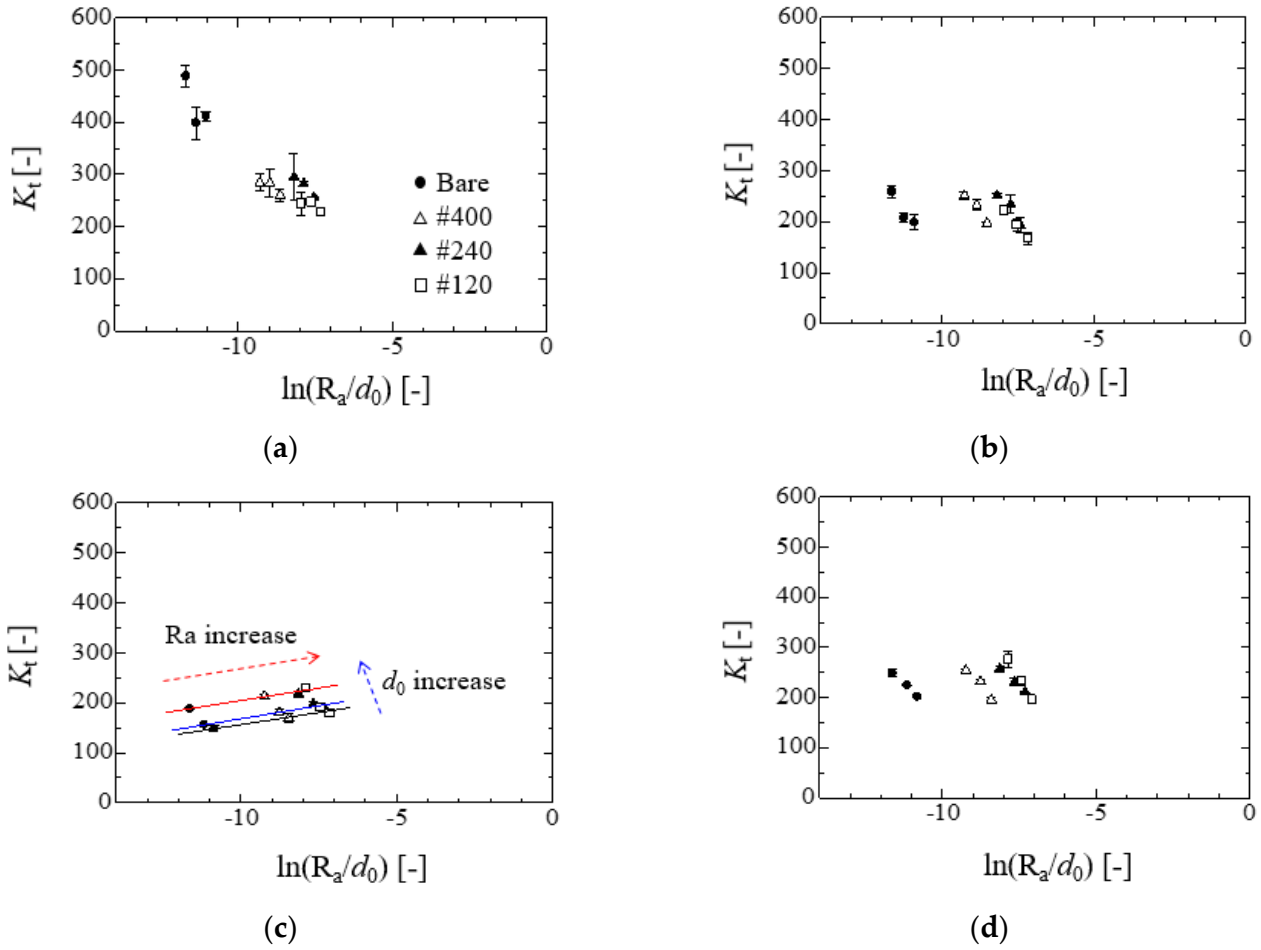

Figure 9. Relationship between K_t and ln(Ra/d0): (**a**) 5 wt%; (**b**) 20 wt%; (**c**) 70 wt%; and (**d**) 99.4 wt%. The error indicates two standard deviation (2SD).

However, from the results in the cases from Figure 9b–d, some groups appear, and each trend exhibits complex linear relation as the ethanol concentration increases. The trend cannot be depicted by a single linear line. This tendency cannot be considered in the model of Equation (4) because the model was mainly developed on the basis of the results in the narrow range of the droplet size. The groups indicate the effects of the droplet size and the solid surface condition on the splashing. Furthermore, the effect of the surface roughness/wettability on the splashing condition becomes small as the ethanol concentration increases because there are no large differences in the K_t values against each group. Considering the tendency in Figure 9, it is found that each linear group in each liquid case has a similar gradient, which corresponds to the coefficient D of Equation (4). This may indicate the dependency of the kinds of liquid. In addition, judging from the

figures such as Figure 9c, the intercept in Equation (4) would be influenced by both the kinds of liquid and the droplet volume. Figure 10 shows the evaluation results for the coefficients C and D of Equation (4) in the present experiment. Here, the values C and D for each liquid are evaluated by focusing on the linearity for each droplet volume represented by the red dashed arrow as Figure 9c. The parameter K_t (=$(We/Oh)^{1/2}$) of Equation (4) can be alternatively represented by the expression $(ReFr)^{1/2}(d_0/l_{cap})^{1/2}$, where Fr (=$u/(gd_0)^{1/2}$) is the Froude number and d_0 is the initial droplet diameter. Therefore, the parameter $(d_0/l_{cap})^{1/2}$ can also be an important factor to determine the parameter K_t. In addition, the coefficient C exhibited the droplet volume dependency. Thus, the value for the coefficient C is divided by $(d^*)^{1/2}$ in order to consider the volume effect: d^* is d_0/l_{cap}. The liquid properties are also an important factor for the splashing behavior [19]. Therefore, the horizontal axis represents the Oh number evaluated by the capillary length of the liquid ($Oh_{cap} = \mu_l / (\rho_l \, l_{cap} \, \sigma_{lg})^{1/2}$). The value of Oh_{cap} purely expresses the liquid property. From Figure 10a,b, it is found that the values of $C/(d^*)^{1/2}$ and D almost take constant value in each liquid. From the results in Figure 10c,d, it is found that the values of $C/(d^*)^{1/2}$ and D exhibit a potential for the correlation of $\alpha Oh_{cap}{}^{n} + \beta$ where the α and β are the arbitral fitting parameters. From above discussion, the coefficients C and D in Equation (4) can be expressed by the following relation (Section S2 in the Supplementary Materials):

$$C = \left(\frac{C_1}{Oh_{cap}^{0.170}} + C_2 \right) \sqrt{\frac{d_0}{l_{cap}}} \tag{10}$$

$$D = \frac{D_1}{Oh_{cap}^{0.170}} + D_2 \tag{11}$$

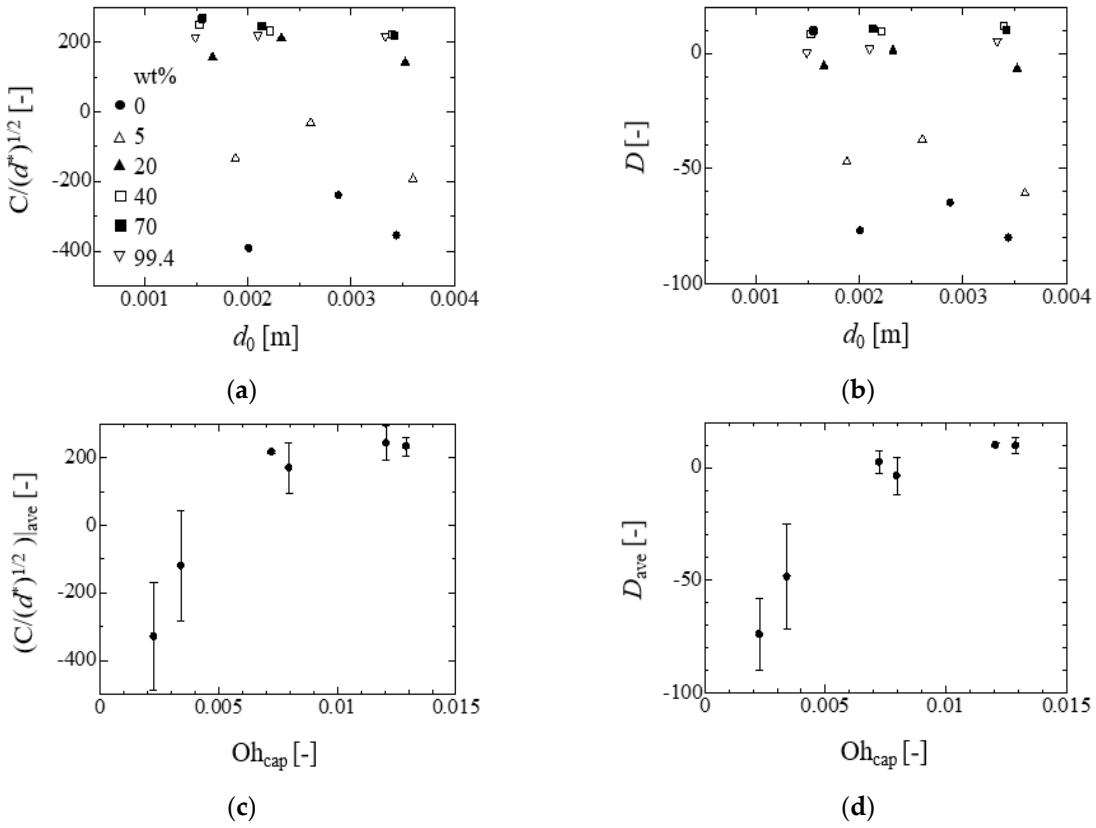

Figure 10. Coefficients C and D in Equation (4): size dependences in (**a**) $C/(d^*)^{1/2}$ and (**b**) D; Oh_{cap} dependences in (**c**) averaged $C/(d^*)^{1/2}$ and (**d**) averaged D where each value is averaged among droplet sizes. The error indicates two standard deviation (2SD).

In this relation, C_1, C_2, D_1, and D_2 are the arbitrary fitting parameters that were –528.0, 1319, –91.23, and 198.1, respectively. Figure 11 shows the comparison of K_t in experiment with the K_t evaluated by Equation (4) with Equations (10) and (11). From the result, the predicted values of $K_{t\text{-pre}}$ show relatively good agreement with that of $K_{t\text{-exp}}$.

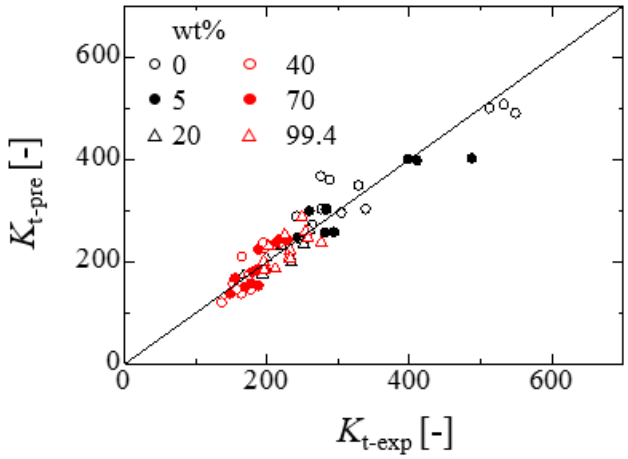

Figure 11. Comparison of $K_{t\text{-exp}}$ with $K_{t\text{-pre}}$ in each liquid.

In the above discussion, the referenced models such as Equations (2) and (4) are relatively well-organized equations. Thus, a simpler approach can be applied to the present result and discussed. Figure 12 shows the relationship between Oh and the critical Re_c for all droplets impinging on each solid substrate. This kind of trend can be correlated by the relation $OhRe^n = C_0$ [24]. In fact, the red solid line in Figure 12 is correlated by the following relation (Section S2 in the Supplementary Materials):

$$\ln \mathrm{Oh} = E \ln \mathrm{Re}_c + F \tag{12}$$

In this equation, the coefficients E and F represent the parameters that depend on the surface roughness as follows:

$$\frac{E - E_{\mathrm{bare}}}{E_{\mathrm{bare}}} = E_1 \tanh\left\{ E_2 \left(\frac{f_{\mathrm{rf}} - f_{\mathrm{rf}}^{\mathrm{bare}}}{f_{\mathrm{rf}}^{\mathrm{bare}}} \right) \right\} \tag{13}$$

$$\frac{F - F_{\mathrm{bare}}}{F_{\mathrm{bare}}} = F_1 \tanh\left\{ F_2 \left(\frac{f_{\mathrm{rf}} - f_{\mathrm{rf}}^{\mathrm{bare}}}{f_{\mathrm{rf}}^{\mathrm{bare}}} \right) \right\} \tag{14}$$

In Equations (13) and (14), E_{bare}, F_{bare}, E_1, E_2, F_1, and F_2 are the fitting parameters that were –0.7836, 1.219, 0.6393, 10.25, 3.197, and 10.33, respectively. The correlated solid line shows fairly good agreement with the experimental data. This approach can directly evaluate the critical value such as Re_c.

From the result in the evaluation of Equation (5), it is implied that the ejecting angle of the secondary droplet may be estimated by $\tan\alpha_{\mathrm{mod}}$ which is related to the contact angle, which can be basically expressed by the surface tension of liquid σ_{lg}, the critical surface tension of solid σ_c, and the roughness factor f_{rf} as follows [34,37]:

$$\cos\theta_{\mathrm{app}} = -1 + 2\frac{\sigma_c(f_{\mathrm{rf}})}{\sigma_{\mathrm{lg}}} + \frac{\Gamma(f_{\mathrm{rf}})\mathrm{R}T}{\sigma_{\mathrm{lg}}} \ln\left(\frac{\sigma_{\mathrm{lg}}}{\sigma_c(f_{\mathrm{rf}})} \right) \tag{15}$$

where the R [J/(mol × K)] and T [K] are gas constant and temperature, respectively. σ_c [N/m] and Γ [mol/m^2] which are functions of f_{rf} [34] are the critical surface tension and the amount of adsorption molecules per unit of interfacial area, respectively. The critical surface tension is a measure for the solid surface tension [38]. In addition, the behavior

of the liquid film would be affected by the liquid properties [27]. Therefore, the $\tan\alpha_{mod}$ can be alternatively associated with Oh_{cap} that includes the liquid properties such as the surface tension and viscosity.

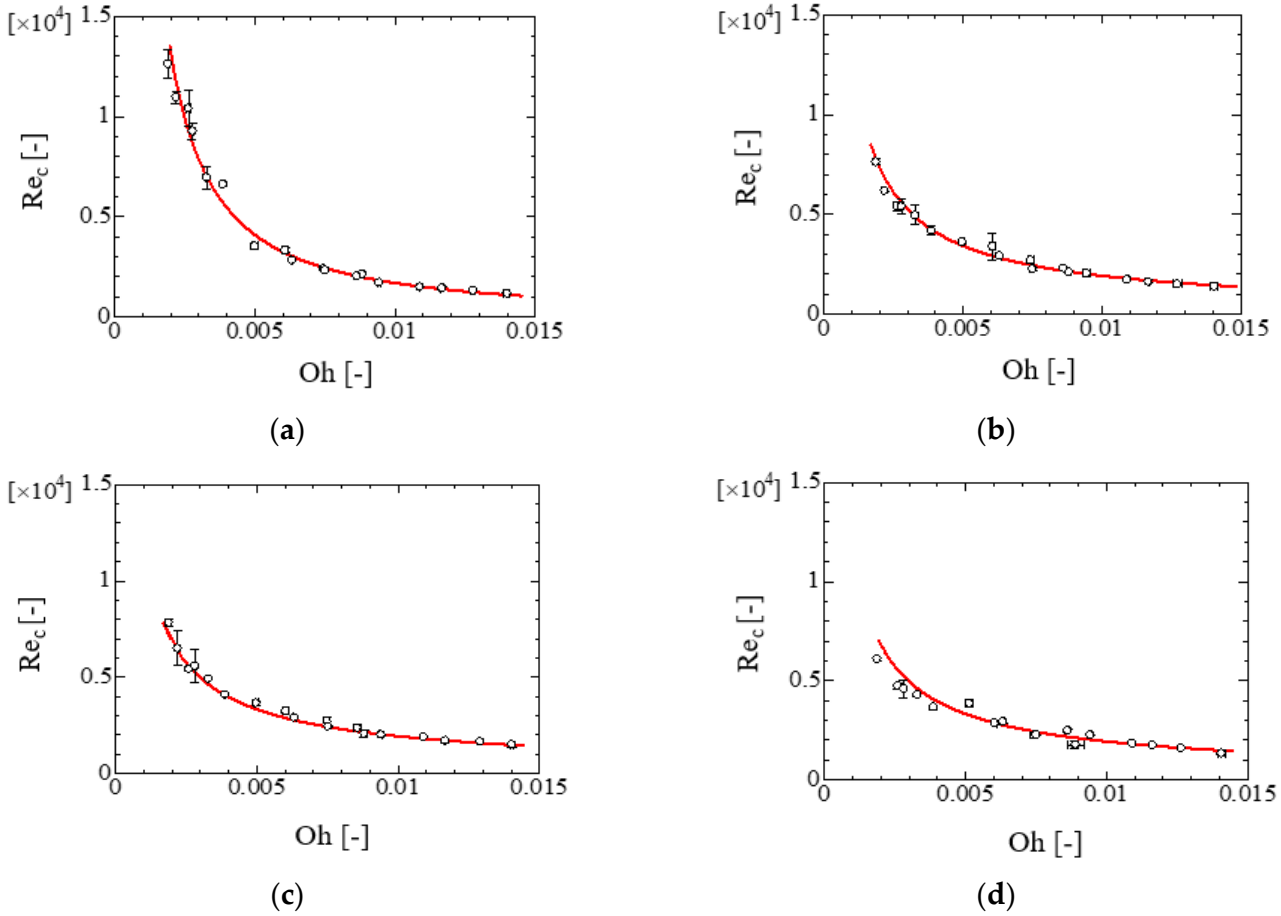

Figure 12. The relationship between Re_c and Oh: (**a**) bare substrate; (**b**) #400 substrate; (**c**) #240 substrate; and (**d**) #120 substrate. The error indicates two standard deviation (2SD).

Here, the result in Figure 10 shows the importance of the Oh_{cap} for the consideration of the liquid properties. In addition, the lift force of the liquid film is related to the slip length at the gas-liquid interface characterized by $Oh^{1/4}$. This would indicate that the liquid film behavior including the lifted angle is also characterized by $Oh^{1/4}$. Actually, the value of the $\tan\alpha_{mod}$ relatively exhibits linearity against ${Oh_{cap}}^{-1/4}$ as shown in Figure 13. Then, if the initial kinetic energy increases, the splashing behavior will change from the prompt to the corona splash where the ejecting angle also increases [32]. This implies the relation $We_c \propto \tan\alpha_{mod}$. Figure 14 shows the relationship between We_c and ${Oh_{cap}}^{-1/4}$. The trend in each solid substrate shows the relatively linear relation between We_c and ${Oh_{cap}}^{-1/4}$. In this figure, ${Oh_{cap}}^{-1/4}$ increases as the ethanol concentration decreases. The trends in the linearity are different depending on the solid substrates. From Figure 7, significant changes in the value of $\cos\bar{\theta}_{ave}$ occur in the cases of 0 wt% and 5 wt% where the hydrophobicity increases. This may imply that the kinetic energy is mainly consumed to disintegrate the droplet because of the decrease in wettability. Eventually, this consideration focusing on the liquid film behavior yields the following simple relation.

$$We_c = \frac{G}{Oh_{cap}^{1/4}} + H \tag{16}$$

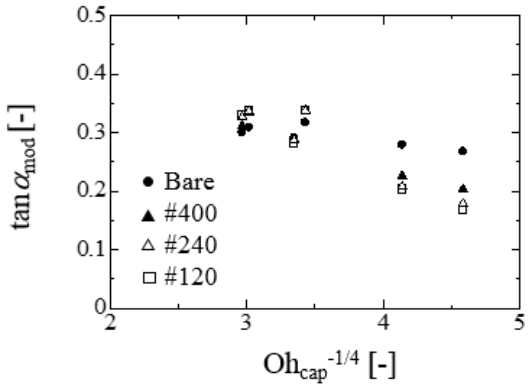

Figure 13. Relationship between $\tan\alpha_{mod}$ and $Oh_{cap}{}^{-1/4}$.

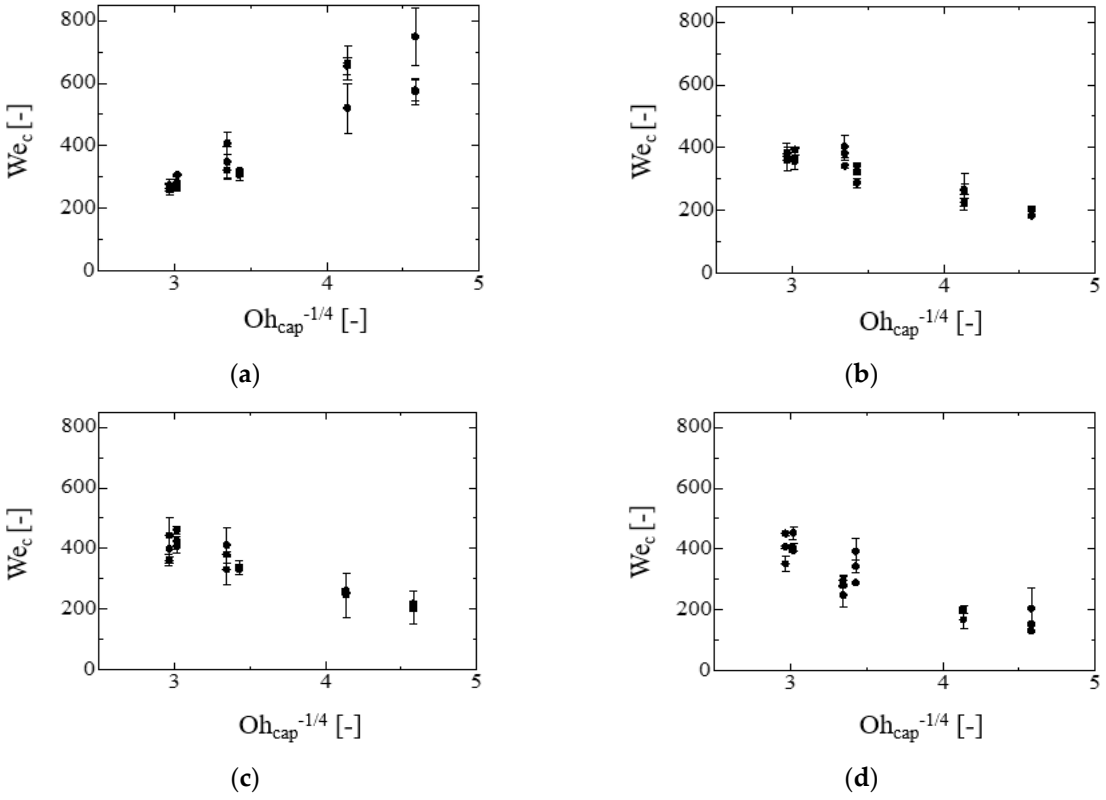

Figure 14. Relationship between We_c and Oh_{cap}: (**a**) bare substrate; (**b**) #400 substrate; (**c**) #240 substrate; and (**d**) #120 substrate.

In this equation, the coefficients G and H represent the parameters that depend on the surface roughness as follows (see Supplementary Materials):

$$\frac{G_{bare} - G}{G_{bare}} = G_1 \tanh\left\{ G_2 \left(\frac{f_{rf} - f_{rf}^{bare}}{f_{rf}^{bare}} \right) \right\} \quad (17)$$

$$\frac{H_{bare} - H}{H_{bare}} = H_1 \tanh\left\{ H_2 \left(\frac{f_{rf} - f_{rf}^{bare}}{f_{rf}^{bare}} \right) \right\} \quad (18)$$

In Equations (17) and (18), G_{bare}, H_{bare}, G_1, G_2, H_1, and H_2 are fitting parameters that were 250.9, –487.7, 1.583, 13.22, 2.720, and 12.87, respectively. Equation (16) considers the effect of the liquid property and the surface roughness on the liquid film behavior by treating G, H, and Oh_{cap} independently.

Figures 15 and 16 show the results of the comparison of the experimental value for the We_c and Re_c with the predicted ones by each model, respectively. Here, in the results for Equation (2), We and Re were re-evaluated on the basis of the initial droplet diameter d_0 as $We = 2We_{RG}$ and $Re = 2Re_{RG}$. From these results, it seems to be found that there are no large differences in accuracies among the models. If anything, the accuracy of the predicted values by Equation (4) is low in both We_c and Re_c. To evaluate the accuracy quantitatively, the relative error $E_{n\text{-}wt\%} = 100 \times |(x_{exp} - x_{pre})/x_{exp}|_{n\text{-}wt\%}$ was calculated in each liquid case: x corresponded to We_c or Re_c. Table 4 shows the accuracy of each model, E_{ave} indicates the averaged values over all the kinds of liquid cases for the relative error $E_{n\text{-}wt\%}$. The error was evaluated in each solid substrate. E_{2SD} indicates the two standard deviation for the errors over all the kinds of liquid cases. From Table 4, it is found that the model for Equation (16) shows the best prediction by considering both the E_{ave} and E_{2SD}. The important point is that the parameter which characterizes the surface condition such as the contact angle or surface roughness is included in each model. In addition, the present results indicated that the critical values such as We_c and Re_c could not be predicted accurately even if the splashing parameter where the We_c and Re_c were included as parameters was well predicted. This may be because other parameters and their combination reduce the error. From the present study, it is found that the Re_c can also be accurately predicted if the We_c can be accurately predicted. From an engineering point of view, this kind of direct prediction would be more useful than the indirect prediction of the splashing parameters such as K_t and K_c. On the other hand, from an academic point of view, the modeling on the basis of the comprehensive concept such as Equation (2) would be important.

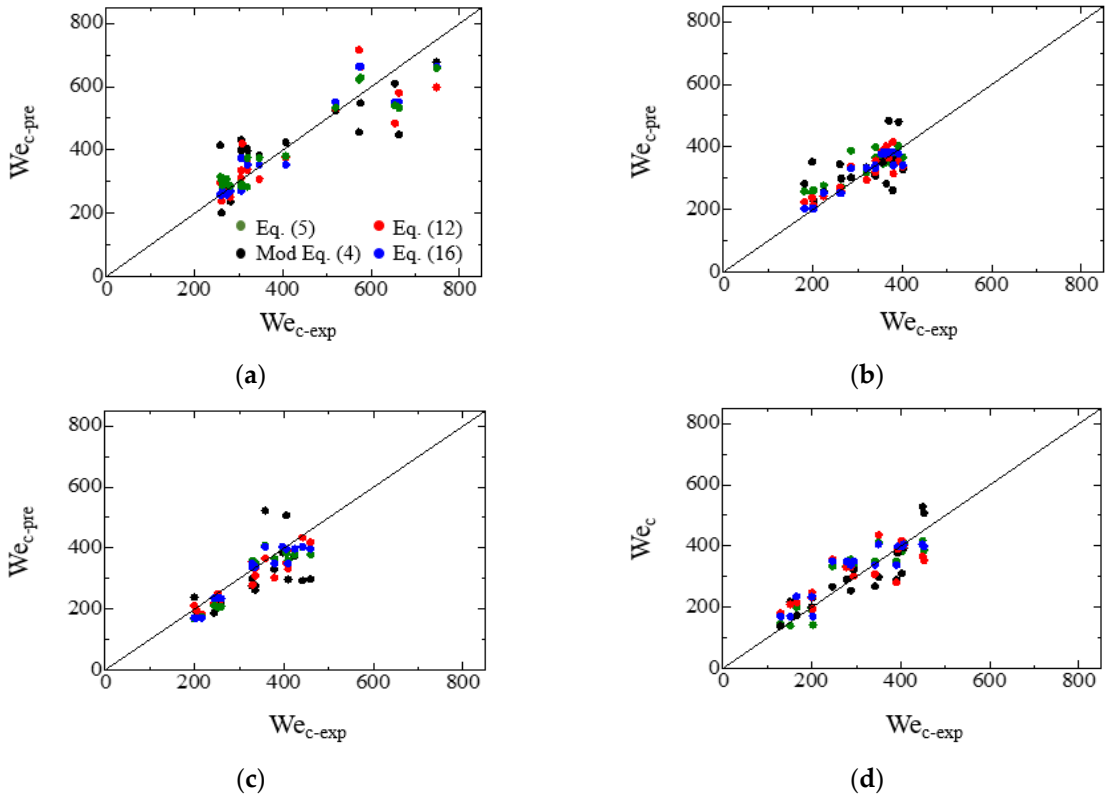

Figure 15. Comparison of experimental value for We_c with the predicted one in each model: (**a**) bare substrate; (**b**) #400 substrate; (**c**) #240 substrate; (**d**) #120 substrate. The green, black, red, and blue symbols are predicted by Equation (5), Equation (4) with Equations (10) and (11), and Equation (12) and Equation (16), respectively.

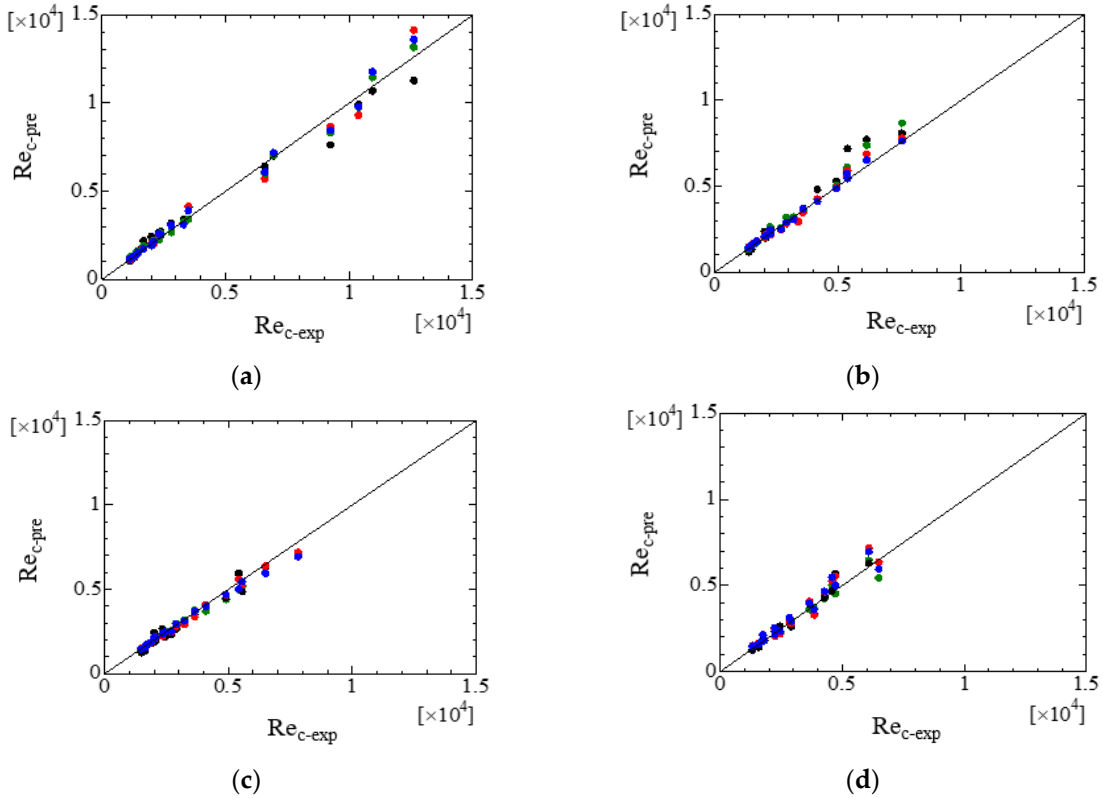

Figure 16. Comparison of experimental value for Re_c with the predicted one in each model: (**a**) bare substrate; (**b**) #400 substrate; (**c**) #240 substrate; and (**d**) #120 substrate. The green, black, red, and blue symbols are predicted by Equation (5), Equation (4) with Equations (10) and (11), and Equation (12) and Equation (16), respectively.

Table 4. Accuracy of each model. E_{ave} indicates the averaged values over all the kinds of liquid cases for the relative error $E_{n\text{-}wt\%} = 100\,|(x_{exp} - x_{pre})/x_{exp}\,|_{n\text{-}wt\%}(\%)$. E_{2SD} indicates the two standard deviation for the errors over all the kinds of liquid cases: x corresponds to We_c or Re_c.

		Bare		#400		#240		#120	
Model	**Error**	**Re**	**We**	**Re**	**We**	**Re**	**We**	**Re**	**We**
Equation (5)	E_{ave}	5.3	10.6	5.4	10.4	6.3	13.1	6.3	12.7
	E_{2SD}	6.0	12.5	10	18.5	7.7	16.5	9.9	20.7
Equation (4) with Equations (10) and (11)	E_{ave}	9.8	20.2	9.6	20.2	11.7	20	6.6	13.1
	E_{2SD}	14.1	30.8	17.2	39	17.7	22.9	10.5	21.5
Equation (12)	E_{ave}	6.3	12.7	5.2	9.9	4.6	8.9	9.0	18.6
	E_{2SD}	9.0	18.5	7.2	12.2	6.8	12.8	12.3	26.4
Equation (16)	E_{ave}	5.3	10.6	2.9	5.8	4.4	8.5	7.7	16
	E_{2SD}	6.7	13.6	4.9	9.9	6.7	12.8	11	24.1

5. Conclusions

Droplet splashing behaviors were experimentally investigated. In the experiment, five kinds of water-ethanol binary mixture liquids were used in order to investigate the effect of the surface tension, viscosity, and wettability on the splashing condition. The effect of the surface roughness of solid substrate on the splashing condition was also considered by polishing the surface of the polycarbonate. Then, the experimental data for the splashing condition were evaluated on the basis of existing models. In the results, it is found that the model proposed by Gordillo and Riboux (Equations (2) and (3)) that focuses on the condition of $We_\varepsilon \leq 1$ relatively showed good agreement with the proposed splashing

condition $K_c \simeq 0.034$ for the bare substrate although there were large discrepancies with respect to the other solid substrates such as #400, #240, and #120 substrates. The K_c evaluated on the basis of the present experimental data exhibited the dependency of the contact angle and $(r^*)^{-1/4}$ ($r^* = r_0/l_{cap}$). In the evaluation based on Equation (4), the splashing condition K_t was found to be related to the Oh_{cap} and d^* ($=d_0/l_{cap}$) in addition to the roughness information R_a. As to a simpler approach for the relation $OhRe^n = C_0$, it is found that the present results also held its relation and the experimental data for the relationship between Re_c and Oh were correlated very well. From the result based on the evaluation in Equation (5), a simple model of the relationship between We_c and Oh_{cap} was proposed by focusing on the liquid film behavior such as the lifted angle of the liquid film. Finally, the accuracy among the models was evaluated by comparing the present experimental values of We_c and Re_c with the predicted ones by each model. The accuracy of the proposed model was the best compared with other models. However, each model indicated the importance of the liquid properties and the solid surface condition. Especially, it is found that the usage of the Oh_{cap} that includes the viscosity effect would be useful for the prediction of the We_c and Re_c. In addition, the result also indicated that the accurate prediction of the splashing parameter did not necessarily make the accurate prediction of the We_c and Re_c. However, from the engineering point of view, the direct and simple approach such as Equation (16) is useful. On the other hand, from the academic point of view, the comprehensive approach could be important to elucidate the mechanism of the droplet behavior.

Supplementary Materials: The following supporting information can be downloaded at: https://www.mdpi.com/article/10.3390/fluids7010038/s1, Section S1: Evaluation for the impingement velocity of droplets, Section S2: Coefficients in Equations (4), (5), (12), and (16), Figure S1: Images for determination of impingement velocity of droplets, Figure S2: Comparison of measured impingement velocity of droplets with analytical results, Figure S3: Relationship between the experimental and the predicted values for the coefficient a and b in Equation (5): (**a**) a vs. f_{rf}; (**b**) b vs. f_{rf}. a and b are predicted by Equations (6) and (7), respectively, Figure S4: Relationship between the experimental and the predicted values for the coefficient E and F in Equation (12): (**a**) E vs. f_{rf}; (**b**) F vs. f_{rf}. E and F are predicted by Equations (13) and (14), respectively, Figure S5: Relationship between the experimental and the predicted values for the coefficient G and H in Equation (16): (**a**) G vs. f_{rf}; (**b**) H vs. f_{rf}. G and H are predicted by Equations (17) and (18), respectively, Figure S6: Example for droplet size dependency of the coefficients C and D in Equation (4) for the case of 70 wt%: (**a**) C vs. d_0; (**b**) D vs. d_0, Figure S7: Comparison of experimental and predicted values: (**a**) coefficient C divided by $(d_0/l_{cap})^{1/2}$; (**b**) coefficient D.

Author Contributions: Conceptualization, Y.Y. and T.K.; data curation, Y.Y.; writing—original draft preparation, Y.Y.; investigation, Y.Y., K.T. and M.Y.; writing—reviewing and editing, Y.Y. and T.K.; methodology, Y.Y. and T.K. All authors have read and agreed to the published version of the manuscript.

Funding: This study was funded in part by JSPS KAKENHI (grant number 17K14590).

Institutional Review Board Statement: Not applicable.

Informed Consent Statement: Not applicable.

Data Availability Statement: The data presented in this study are available in article and Supplementary Material.

Conflicts of Interest: The authors declare no conflict of interest.

References

1. Wijshoff, H. Drop dynamics in the inkjet printing process. *Curr. Opin. Colloid Interface Sci.* **2018**, *36*, 20–27. [CrossRef]
2. Breitenbach, J.; Roisman, I.V.; Tropea, C. From drop impact physics to spray cooling models: A critical review. *Exp. Fluids* **2018**, *59*, 1–21. [CrossRef]
3. Xu, R.; Wang, G.; Jiang, P. Spray cooling on enhanced surfaces: A review of the progress and mechanisms. *J. Elect. Packag.* **2022**, *144*, 010802-1–010802-21. [CrossRef]

4. Guettler, N.; Knee, P.; Ye, Q.; Tiedje, O. Initial droplet conditions in numerical spray painting by electrostatic rotary bell sprayers. *J. Coat. Technol. Res.* **2020**, *17*, 1091–1104. [CrossRef]
5. Geng, L.; Wang, Y.; Wang, Y.; Li, H. Effect of the injection pressure and orifice diameter on the spray characteristics of biodiesel. *J. Traffic Trans. Eng.* **2020**, *7*, 331–339. [CrossRef]
6. Fritz, B.K.; Hoffmann, W.C.; Bagley, W.E.; Kruger, G.R.; Czaczyk, Z.; Henry, R.S. Measuring droplet size of agricultural spray nozzles–measurement distance and airspeed effects. *Atom. Sprays* **2014**, *24*, 747–760. [CrossRef]
7. Yarin, A.L. Drop impact dynamics: Splashing, spreading, receding, bouncing. *Annu. Rev. Fluid Mech.* **2006**, *38*, 159–192. [CrossRef]
8. Manzello, S.L.; Yang, J.C. An experimental investigation of water droplet impingement on a heated wax surface. *Int. J. Heat Mass Transfer* **2004**, *47*, 1701–1709. [CrossRef]
9. Lim, T.; Han, S.; Chung, J.; Chung, J.T.; Ko, S.; Grigoropoulos, C.P. Experimental study on spreading and evaporation of inkjet printed pico-liter droplet on a heated surbstrate. *Int. J. Heat Mass Transfer* **2009**, *52*, 431–441. [CrossRef]
10. Visser, C.W.; Frommhold, P.E.; Wildeman, S.; Mettin, R.; Lohse, D.; Sun, C. Dynamics of high-speed micro-drop impact: Numerical simulations and experiments at frame-to-frame times below 100ns. *Soft Matter* **2015**, *11*, 1708. [CrossRef] [PubMed]
11. Wang, F.; Yang, L.; Wang, L.; Zhu, Y.; Fang, T. Maximum spread of droplet impacting onto solid surfaces with different wettabilities: Adapting a rim-lamella shape. *Langmuir* **2019**, *35*, 3204–3214. [CrossRef]
12. Du, J.; Zhang, Y.; Min, Q. Numerical investigations of the spreading and retraction dynamics of viscous droplets impact on solid surfaces. *Colloids Surf. A Physicochem. Eng. Aspects* **2021**, *609*, 125649. [CrossRef]
13. Lunkad, S.F.; Buwa, V.V.; Nigam, K.D.P. Numerical simulations of drop impact and spreading on horizontal and inclined surfaces. *Chem. Eng. Sci.* **2007**, *62*, 7214–7224. [CrossRef]
14. Börnhorst, M.; Cai, X.; Wörner, M.; Deutschmann, O. Maximum spreading of urea water solution during drop impingement. *Chem. Eng. Technol.* **2019**, *42*, 2419–2427. [CrossRef]
15. Yonemoto, Y.; Kunugi, T. Analytical consideration of liquid droplet impingement on solid surfaces. *Sci. Rep.* **2017**, *7*, 2362. [CrossRef]
16. Ukiwe, C.; Kwok, D.Y. On the maximum spreading diameter of impacting droplets on well-prepared solid surfaces. *Langmuir* **2005**, *21*, 666–673. [CrossRef] [PubMed]
17. Du, J.; Wang, X.; Li, Y.; Min, Q. Maximum spreading of liquid droplets impact on concentric ring-textured surfaces: Theoretical analysis and numerical simulation. *Colloids Surf. A Physicochem. Eng. Aspects* **2021**, *630*, 127647. [CrossRef]
18. Yonemoto, Y.; Kunugi, T. Universality of droplet impingement: Low-to-high viscosities and surface tensions. *Coatings* **2018**, *8*, 409. [CrossRef]
19. Almohammadi, H.; Amirfazli, A. Droplet impact: Viscosity and wettability effects on splashing. *J. Colloid Int. Sci.* **2019**, *553*, 22–30. [CrossRef]
20. Cossali, G.E.; Coghe, A.; Marengo, M. The impact of a single drop on a wetted solid surface. *Exp. Fluids* **1997**, *22*, 464–472. [CrossRef]
21. Brown, A.L.; Jepsen, R.A.; Yoon, S.S. Modeling large-scale drop impact: Splash criteria and droplet distribution. In Proceedings of the ILASS Americas, 21th Annual Conference on Liquid Atomization and Spray Systems, Orlando, FL, USA, 18–21 May 2008.
22. Gipperich, A.; Lembach, A.N.; Roisman, I.V.; Tropea, C. On the splashing thresholds of a single droplet impacting onto rough and porous surfaces. In Proceedings of the ILASS Europe 2010, 23rd Annual conference on liquid atomization and spray systems, Brno, Czech Republic, 6–8 September 2010.
23. Kittel, H.M.; Alam, E.; Roisman, I.; Tropea, C.; G.-Roisman, T. Splashing of a Newtonian drop impacted onto a solid substrate coated by a thin soft layer. *Colloids Surf. A Physicochem. Eng. Aspects* **2018**, *553*, 89–96. [CrossRef]
24. Mundo, C.; Sommerfeld, M.; Tropea, C. Droplet-wall collisions: Experimental studies of the deformation and breakup process. *Int. J. Multiph. Flow* **1995**, *21*, 151–173. [CrossRef]
25. Roisman, I.V.; Lembach, A.; Tropea, C. Drop splashing induced by target roughness and porosity: The size plays no role. *Adv. Colloid Int. Sci.* **2015**, *222*, 615–621. [CrossRef]
26. Quetzeri-Santiago, M.A.; Castrejon-Pita, A.A.; Castrejon-Pita, J.R. The effect of surface roughness on the contact line and splashing dynamics of impacting droplets. *Sci. Rep.* **2019**, *9*, 15030. [CrossRef]
27. Riboux, G.; Gordillo, J.M. Experiments of drops impacting a smooth solid surfaces: A model of the critical impact speed for drop splashing. *Phys. Rev. Lett.* **2014**, *113*, 024507. [CrossRef]
28. Garcia-Geijo, P.; Quintero, E.S.; Riboux, G.; Gordillo, J.M. Spreading and splashing of drops impacting rough substrates. *J. Fluid Mech.* **2021**, *917*, A50. [CrossRef]
29. Gordillo, J.M.; Riboux, G. A note on the aerodynamic splashing of droplets. *J. Fluid Mech.* **2019**, *871*, R3. [CrossRef]
30. Quetzeri-Santiago, M.A.; Yokoi, K.; Castrejon-Pita, A.A.; Castrejon-Pita, J.R. role of the dynamic contact angle on splashing. *Phys. Rev. Lett.* **2019**, *122*, 228001. [CrossRef]
31. Uchida, H. JSME Data Book: Thermophysical Properties of Fluids. *JSME* **1983**, 473–474. (In Japanese)
32. Zhang, H.; Zhang, X.; Yi, X.; He, F.; Niu, F.; Hao, P. Effect of wettability on droplet impact: Spreading and splashing. *Exp. Therm. Fluid Sci.* **2021**, *124*, 110369. [CrossRef]
33. Tang, C.; Qin, M.; Weng, X.; Zhang, Z.; Zhang, P.; Li, J.; Huang, Z. Dynamics of droplet impact on solid surface with different roughness. *Int. J. Multiph. Flow* **2017**, *96*, 56–69. [CrossRef]

34. Yonemoto, Y.; Tomimitsu, I.; Shimizu, K.; Kunugi, T. Wettability model for water-ethanol binary mixture droplet on roughened low-surface energy solids. *Int. J. Multiph. Flow* **2021**, *137*, 103569. [CrossRef]
35. De Goede, T.C.; de Bruin, K.G.; Shahidzadeh, N.; Bonn, D. Predicting the maximum spreading of a liquid drop impacting on a solid surface: Effect of surface tension and entrapped air layer. *Phys. Rev. Fluids* **2019**, *4*, 053602. [CrossRef]
36. De Gennes, P.G. Wetting: Statics and dynamics. *Rev. Mod. Phys.* **1985**, *57*, 827–863. [CrossRef]
37. Yonemoto, Y.; Kunugi, T. Experimental and theoretical investigation of contact-angle variation for water-ethanol mixture droplets on a low-surface-energy solid. *Int. J. Heat Mass Transfer* **2016**, *96*, 614–626. [CrossRef]
38. Yonemoto, Y.; Kunugi, T. Estimating critical surface tension from droplet spreading area. *Phys. Lett. A* **2020**, *384*, 126218. [CrossRef]